Single pixel imaging: a study of the illumination system position

Author: Guillem Barta Gonzàlez*
Facultat de Física, Universitat de Barcelona, Diagonal 645, 08028 Barcelona, Spain.

Advisor: David Maluenda Niubó

Abstract: Single-pixel cameras use a single light sensor, combined with a projection of illumination patterns, to scan an object and reconstruct an image. In this report, the effect of the position of the illumination system is studied, and a novel method for medical imaging is proposed using single-pixel imaging.

I. INTRODUCTION

Conventional cameras, like those of smartphones, use lenses to project an image on a two-dimensional array of detectors, known as charge-coupled devices (CCD). These detectors are sensitive to a certain range of electromagnetic radiation, generally visible light for common photography.

Nowadays, a wide variety of sensors and lenses are available at a competitive price, since they can cover most of today's photography needs. However, applications that need to work with radiation out of the visible, like SWIR, IR, UV, or X-ray, have complex treatment and require expensive lenses, complex illumination systems, and sensors in the desired wavelengths. It is in these situations that single detectors excel over CCDs. For instance, Atomic Force Microscope (AFM) is a clear example of recovering high-resolution images with a single sensor; the AFM uses a highly sensitive thin spike to scan a material's surface to recover an atomic-resolution image. Therefore, the research for alternatives to reduce cost and complexity such as single-pixel imaging techniques is justified.

The objective of this thesis is to study how the illumination system affects the reconstructions on single-pixel cameras. The paper is structured as follows; sections 2 and 3 provide background information of single-pixel techniques, section 4 presents the used hardware and the experiment setup, section 5 explains how the experiment was carried out, sections 6 and 7 contain the results, the discussion, and the conclusions, and section 8 proposes future work on medical imaging.

II. PREVIOUS WORKS

The concept of single-pixel (SP) cameras was first proposed in a dual photography paper published by Sen et al. in 2005 [1], in which an image was reconstructed using a single photoresistor to detect backscattered light from the structured illumination provided by a projector. One year later, in 2006, Candes & Tao published a paper on compressive sampling [2], which aims to represent digital signals with fewer measurements than the Nyquist-Shannon theorem suggests, describing a digital image in fewer terms without compromising resolution. In 2008, a paper combining both techniques was published by Duarte et al. named "Single-pixel imaging via compressive sampling" [3], which would later become the foundation for SP imaging techniques.

In the last decade, a handful of techniques have been developed, offering imaging alternatives and novel methods out of the visible spectrum [10]. In the few months after Duarte's paper, applications on Terahertz SP imaging [4, 6] were already emerging, followed by SP implementation on X-ray diffraction [7], Telescopic Compressive imaging [8], video recording using ML [9], and recently, in 2023, a novel technique using Single-Photon imaging [12]. Depending on the illumination-detection system these techniques can be divided into two big groups: *Structured illumination* (SI) is based on the projection of patterns onto the object of interest, and *Structured detection* (SD) spatially filters the light arriving at the detector. Both systems reconstruct the image using a single detector, however, it is SD systems that are commonly known as *single-pixel cameras*, while SI systems are usually referred to as *Computational Ghost Imaging* [5]. These last ones correspond to this paper's experiment, and they are also capable of depth-perception thanks to the accurate measurement of the signal's time-of-flight.

III. SINGLE-PIXEL & COMPRESSIVE IMAGING

Let's get back to the AFM for a better understanding: its sensor scans one position at a time, registering a single value in each measurement. We can obviously follow this process to recover an image, by illuminating one position of a scene at a time, storing the pixel value of each position with a single detector. In SP imaging, the illumination is in the form of orthonormal patterns, and

*Electronic address: guillemoi2011@gmail.com

it can be mathematically represented by the weighted sum of an orthonormal vector basis, where the vectors $\mathbf{M_i}$ correspond to the illumination patterns and their coefficients $\alpha_\mathbf{i}$ to the measured intensities:

$$\mathbf{I} = \sum_{i=1}^{N} \alpha_i \mathbf{M}_i \tag{1}$$

Even though it is not applied in this experiment, it is interesting to note that the vectors from a Fourier or Walsh-Haddamard (WH) basis would have different pattern weights, as in nature frequencies with different amplitudes, so that least relevant patterns can be spared. This way, a fair reconstruction of the scene is recovered within a margin of error, and fewer than N^2 measurements are needed to form an NxN image. This procedure corresponds to the previously discussed compressive sampling [2, 3] technique, but will not be used in this experiment.

A. Walsh-Haddamard matrices

Following the Master's thesis work from Libe López [11], the Walsh-Haddamard (WH) set has been used for the projection of patterns, which correspond to the vector basis. A mathematical explanation follows:

A 2^k-order Haddamard matrix H_{2^k} can be obtained by iterating the following Kronecker product:

$$H_{2^k} = \begin{pmatrix} 1 & 1 \\ 1 & -1 \end{pmatrix} \otimes H_{2^{k-1}} = \begin{pmatrix} H_{2^{k-1}} & H_{2^{k-1}} \\ H_{2^{k-1}} & -H_{2^{k-1}} \end{pmatrix} \tag{2}$$

A 2^k-order Walsh-Haddamard base of 2D matrices is obtained from the Haddamard H_{2^k} matrix by crossing its rows and columns, which contain Walsh functions, as seen in Figure 1 *(b)*. Walsh functions are binary 1D orthonormal vectors characterized by their sequence, which is the number of changes from 1 to -1 (purple to yellow).

(a) (b) (c)

FIG. 1: (a) is the Haddamard matrix H_8, (b) is the same matrix ordered in ascending sequence (left to right), and (c) is the WH matrix obtained by crossing the 2nd row with the 8th column of the H_8 matrix (b), which are the Walsh functions with sequence 1 and 7, respectively. Purple squares have value -1 and yellow squares have value +1.

IV. EXPERIMENT SETUP

In the experiment, a projector is used to illuminate the scene, and a digital camera to measure light intensity. The process is governed through a Python script, with the projector and camera connected by HDMI and USB to the computer, respectively. Though the project originally used a Pi Camera attached to a Raspberry Pi connected by WiFi, it was later replaced by an IDS camera connected by cable for speed reasons. The different setups of the experiment are shown in Figure 2 and a description of the hardware is provided below.

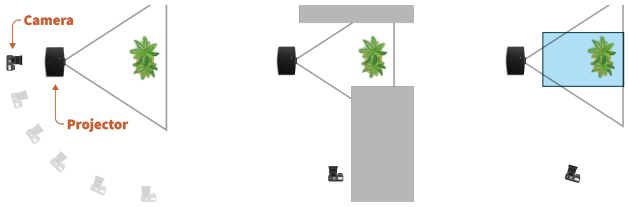

(a) (b) (c)

FIG. 2: Top views of the three setup variations of the experiment: (a) shows a direct observation for different setups (Notice the different positions of the camera on the translucent images), (b) shows the sketch for the indirect observation, and (c) depicts the observation through turbid media.

Projector: A JAVODA P8 Mini DLP commercial projector has been used. In the SP imaging scheme, it plays the role of the light source and the spatial modulator. It provides a 100-lumen 1080p video projection at 60 fps, in the visible spectrum.

Sensor: The initial WiFi variant of the experiment featured a Raspberry Pi Zero 2 W to control a Pi Camera Module 2 sensor and send data through WiFi. This connection comes, however, with the need for a server to host the communication, and unpredictable time delays on data transfer, which is inconvenient for high-speed conditions. With this sensor, a maximum of 5 fps were achieved, above which the reconstructions were messed up by desynchronization problems.

Synchronization is an important aspect, since measurement time rapidly grows with resolution, and high-speed operating systems are required. In the final version of the experiment, an IDS Imaging U3-3270LE-M-GL sensor is used, since it can provide a stable 30 measures per second and the setup is much simpler. The sensor also features an API, which allows the computer to control it directly through USB 3, without the need for Raspberry Pi or a hosting server.

Lens: A Raspberry Pi lens model SC0123 is attached to the senor's chassis (Both cameras support the C-mount of the lens). Even though a lens is not strictly

needed, it helps to regulate the direction and intensity of the rays arriving at the sensor.

Conroller: For both options (wifi/cable), the camera-projector system is controlled by a Python script, which can be found at this GitHub directory and the libraries used are: PiCamera for the Raspberry Pi with WiFi, IDS_camera_interface for the USB camera API, and OpenCV for the matrix projection. The code also creates WH matrices as they are shown, so that there is no need to store them in any computer files.

V. EXPERIMENTAL PROCEDURE

The objective of the experiment is to study how the position of the illumination system affects the formation of images on the structured illumination (SI) [5] scheme. However, this experiment deviates from state-of-the-art SI techniques; these tend to use Digital Micro-mirror Devices (DMD) to reflect the incoming light of a pulsed laser, which allow for modulating the phase of the reflected wave to project ±1 values simultaneously. In this case, the projector only allows for amplitude modulation (and so does the sensor), which means that the values that it will be showing are either 1 (white light) or 0 (no light). To show -1 values the ±1 matrices are projected separately, illuminating, for example, where the yellow squares are on Figure 1 *(c)* and then where the purple ones are. However, this doubles the number of patterns shown, and for a NxN reconstruction, $2N^2$ measurements have to be taken.

Therefore, it is important to synchronize each measure with its projection, and that is no easy task at high speed. For every intensity measure, the code sends the projector the (i,j) WH matrix and retrieves the last frame from the camera buffer, approximately at the same time. Then, an average of the image taken is computed, and multiplied by the projected pattern, as in equation 1. However, a delay from the camera with respect to the projector was noticed when testing the code, wrongly correlating values. Hence, a correction value "delay" has been added to the multiplication procedure, to line up the multiplication of every matrix with its back-scattered intensity.

VI. RESULTS AND DISCUSSION

A. Resolution and speed

For the first reconstructions, different image resolutions were tested with the direct view setup (a) on Figure 2, with the camera aligned with the object and the projector. The results are shown in Figure 3. As observed, the noise grows with the spatial resolution, and it seems to be concentrated on the lower part of the image. This is because the set of WH matrices shown changes faster on the lower parts, which can be solved by decreasing a bit the acquisition speed.

(a) 16x16 (b) 32x32 (c) 64x64

FIG. 3: Gray-scale reconstructions with the direct view setup (Figure 2-*a* opaque camera). The 16x16 image took 30 seconds to reconstruct, the 32x32 took 2 minutes, and the 64x64 took 8 minutes (approx).

Indeed, capture time is related to resolution, and it is expressed through equation 3.

$$t = \alpha \cdot \frac{2N^2}{fps} \tag{3}$$

Where t is the capture time, N is the resolution (in pixels), fps stands for "frames per second", $\alpha > 1$ is an adimensional factor that reflects the overall delay induced in the measurements by the hardware, which is $\alpha = 1.8$ for this particular setup, and the multiplying factor 2 accounts for the separate projection of ±1 matrices,

B. Camera displacement

To test the dependence of the camera position, different angles of the camera-projector were tested, as seen in Figure 2 (a) with the transparent cameras. The results are presented in Figure 4.

In the reconstructions, it seems that the illumination comes from the camera, while the perspective remains the same. This is expected from eq 1, since the the camera gathers more intensity from the parts that it is directly seeing, while the position of the WH projections remains constant. The most interesting example is the 90^{o} case (Figure 4-*f*) since, even if the camera isn't able to directly see parts of the object, it effectively reconstructs them. This phenomenon is explained by the reflection of these hidden areas on parts that the camera is seeing, which then contribute to the total intensity, giving information about out-of-sight parts through the weighting of WH matrices.

(a) 0º (b) 15º (c) 30º

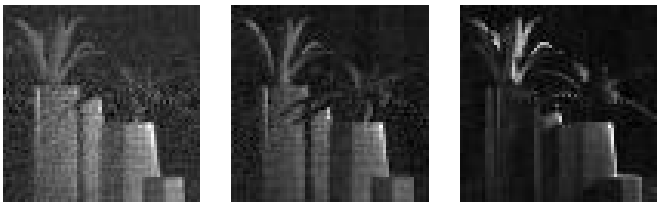

(d) 45º (e) 60º (f) 90º

FIG. 4: 64x64 reconstructions for different angles, with the camera displacement setup (Figure 2-*a* translucent cameras).

C. Scattering

To test the reconstructions of images without directly receiving light from the object, two setups were tested, receiving the reflected light of the object on a wall nearby and a close ceiling, at 10cm and 20cm from the object, respectively. The wall-reflection setup is schemed in Figure 2 (b), the ceiling-reflection setup is similar, but the camera points at at a ceiling over the object. Both reconstructions are shown in Figure 5.

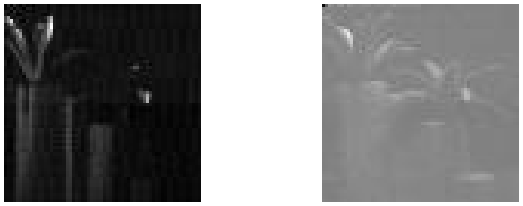

(a) (b)

FIG. 5: 64x64 reconstructions with the camera pointing at a nearby wall (a), and a close ceiling (b). With the reflection setup shown in Figure 2-*b*.

The object is now completely hidden from the camera, yet, the object can be imaged. Both reconstructions seem to be illuminated from the surfaces that the camera is pointed to, but the perspective is, still, that of the projector. This is explained by the same phenomenon that allows hidden parts of the object to be imaged in Figure 4-*f*. On the other side, intensity and contrast have also decayed since the camera is just registering a small part of the scattered light from the object, and the SNR (Signal-to-Noise Ratio) is lower. This effect is even more significant in the ceiling case (b) because the reflecting surface is further from the object.

D. Attenuation

To conclude the study, attenuation effects are tested by reconstructing images that are illuminated through transparent water and through a turbid media (water with a few drops of milk) with the aquarium setup (Figure 2-*c*). Images taken directly with the camera and with the SP technique are shown in Figure 6 for comparison.

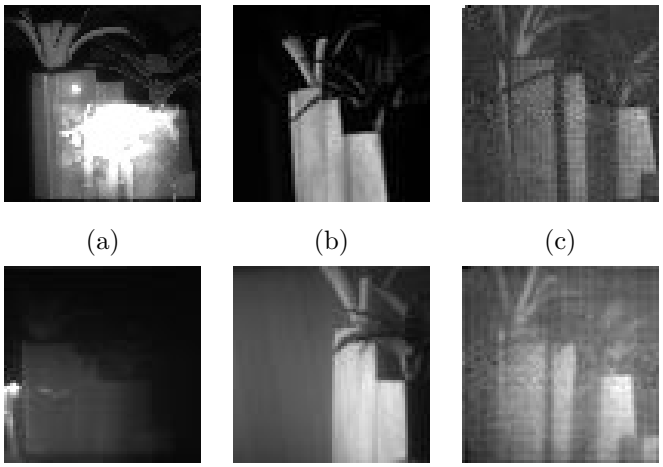

(a) (b) (c)

(d) (e) (f)

FIG. 6: The first row (a,b,c) corresponds to transparent water and the second row (d,e,f) to turbid media. The first column (a,d) corresponds to downscaled images taken directly with the camera at 0º, (b,e) to downscaled images taken directly by the camera at 80º, and (c,f) to SP reconstructions taken from the positions of (b,e), taken also at 80º. All the images are 64x64.

On the one hand, images taken from the front, at 0º, are severely affected by reflection on the glass walls and dispersion, note that the one taken in turbid media (d) is almost indiscernible. On the other hand, SP reconstructions taken from the side, at 80º, did a fairly good job, and the object is discernible in both cases (c,f). However, a photo taken from that same position has better contrast (b,e).

VII. CONCLUSIONS

On the one hand, capture times are predicted by equation 3, but the current setup is not fast enough for it to have a useful application. On the other side, SP cameras have proven to be an alternative to CCDs in

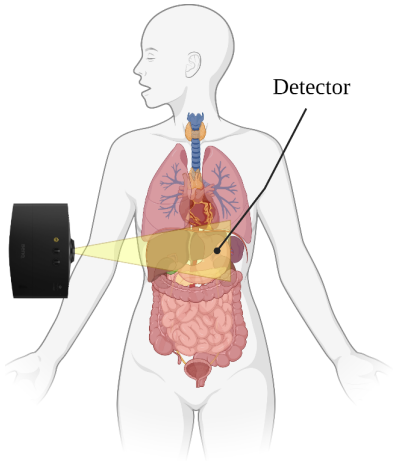

FIG. 7: Example of SP imaging of a kidney. This is a draft; the detector and projector would need more complex setups.

certain scenarios, where the object is out of sight, but direct illumination of the object is possible. Reconstructions in SP imaging have been demonstrated to present the perspective of the projector and the illumination from the detection point. This could have implications in the automotive industry, where self-driving cars are taking the spot, and all kinds of detection systems have to be considered.

VIII. FUTURE WORK

Also, attenuation through turbid media could be of relevance in situations where detection can be carried closer to the object of interest than the illumination system. For example in medical imaging, SP applications could have some advantages over the actual imaging techniques (PET, SPECT, X-ray) that work with frequencies out of the visible. Some advantages could include cheaper equipment because of the single detector reduced cost, and a lower dose per projected matrix because of the fractionation nature of SP imaging. In Figure 7 a proposed example is given: a kidney is imaged with SP techniques, and an image from the projector's perspective would be obtained.

Acknowledgments

Thanks to Dr. Maluenda Niubó for his constant support and to my family for the opportunities they provided me to study for this degree.

[1] Pradeep Sen et. al. 2005. Dual photography. ACM Trans. Graph. 24, 3 (July 2005), 745–755.
[2] E. J. Candes and T. Tao, "Near-Optimal Signal Recovery From Random Projections: Universal Encoding Strategies?", in IEEE Transactions on Information Theory, vol. 52, no. 12, pp. 5406-5425, Dec. 2006.
[3] M. F. Duarte et al., "Single-pixel imaging via compressive sampling", in IEEE Signal Processing Magazine, vol. 25, no. 2, pp. 83-91, March 2008,
[4] Wai Lam Chan et. al., A single-pixel terahertz imaging system based on compressed sensing. Appl. Phys. Lett. 22 September 2008; 93 (12): 121105.
[5] Y. Bromberg et. al., "Ghost imaging with a single detector", Phys. Rev. A 79(5), 053840 (2009).
[6] David Shrekenhamer, Claire M. Watts, and Willie J. Padilla, "Terahertz single pixel imaging with an optically controlled dynamic spatial light modulator", Opt. Express 21, 12507-12518 (2013)
[7] Joel Greenberg et. al. "Compressive single-pixel snapshot x-ray diffraction imaging", Opt. Lett. 39, 111-114 (2014)
[8] Yu, WK., Yao, et al. Complementary compressive imaging for the telescopic system. Sci Rep 4, 5834 (2014).
[9] Higham, C.F., Murray-Smith, et al. Deep learning for real-time single-pixel video. Sci Rep 8, 2369 (2018).
[10] Graham M. Gibson, et. al., "Single-pixel imaging 12 years on: a review", Opt. Express 28, 28190-28208 (2020)
[11] Libe López Arandia, "Single-pixel imaging approach to the Non-Line-of-Sight problem" Master's thesis, 20 July 2022.
[12] Wang, Y., et al. Mid-infrared single-pixel imaging at the single-photon level. Nat Commun 14, 1073 (2023).